Supplement of The Cryosphere, 19, 173–200, 2025
https://doi.org/10.5194/tc-19-173-2025-supplement

The Cryosphere Open Access EGU

Supplement of

Surface processes and drivers of the snow water stable isotopic composition at Dome C, East Antarctica – a multi-dataset and modelling analysis

Inès Ollivier et al.

Correspondence to: Inès Ollivier (ines.ollivier@uib.no)

Supplementary materials

S1 Conversion of RH_{wrtl} to RH_{wrti}

As in Genthon et al. (2017) and Vignon et al. (2022), we use the combination of the three parameters measured simultaneously by the modified HMP155 (T_{heat}, T_{amb} and RH_{wrtl}) to recalculate RH_{wrti}. This method assumes that the partial vapor pressure of water vapor is the same whether the air sampled by the sensor is heated or not. RH_{wrti} is computed as follows:

$$RH_{wrti} = \frac{RH_{wrtl} * p_{sat,l}(T_{heated})}{p_{sat,i}(T_{ambient})} \qquad \text{(S1)}$$

with $p_{sat,l}$ and $p_{sat,i}$ the equations for saturation vapor pressure as a function of temperature from Murphy and Koop (2005) (their Eq. 7 and 10) and RH_{wrtl}, T_{heated} and $T_{ambient}$ given by sensor (see also Fig. 1 in Genthon et al., 2022).

S2 Calculation of standard error of the mean (SEM) and 95% confidence interval (Student t-test)

The standard error of the mean is computed as follows:

$$SEM = \frac{std}{\sqrt{N^*-1}} \qquad \text{(S2)}$$

The mean values are given with the 95% confidence interval (Student t-test) computed as follows:

$$\mu = \bar{x} \pm t_c . \frac{SEM}{\sqrt{N^*-1}} \qquad \text{(S3)}$$

In both Eq. (S2) and (S3), N* is computed as in Bretherton et al. 1999:

$$N^* = N . \frac{(1-r(\Delta t)^2)}{(1+r(\Delta t)^2)} \qquad \text{(S4)}$$

with $r(\Delta t)^2$ from the autocorrelation function (ACF) plots for each variable. As an example, for the $\delta^{18}O$ in the surface snow, $r(\Delta t)^2 = 0.66^2$ (correlation coefficient at lag 1, red dots in Fig. S1).

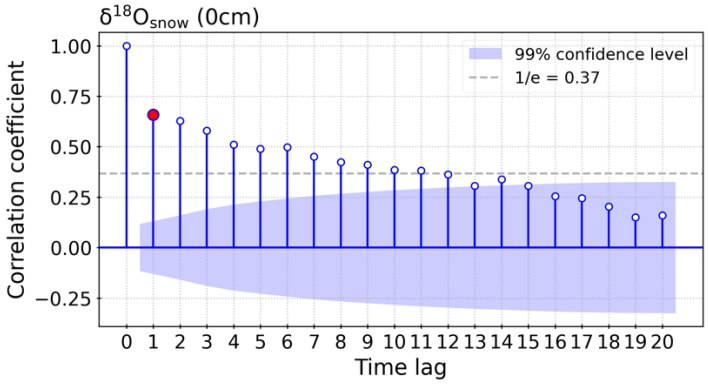

Figure S1. Autocorrelation function for $\delta^{18}O$ in the surface snow.

Table S1 summarizes the values for N* and t_c for each variable used to calculate the SEM and the 95% confidence interval.

Table S1. Summary of N* and Student t-test t_c values for each variable.

	N*	t_c
Precipitation $\delta^{18}O$ (observations)	244	1.97
Precipitation d-excess (observations)	572	1.964
Precipitation (excl. samples with dxs < 0) $\delta^{18}O$ (observations)	246	1.97
Precipitation (excl. samples with dxs < 0) d-excess (observations)	550	1.964
Snow surface $\delta^{18}O$ (observations)	193	1.972
Snow surface d-excess (observations)	256	1.969
Snow subsurface $\delta^{18}O$ (observations)	354	1.967
Snow subsurface d-excess (observations)	393	1.966
Precipitation $\delta^{18}O$ (ECHAM6-wiso)	479	1.965
Precipitation d-excess (ECHAM6-wiso)	1069	1.96

S3 Snow isotopic composition of individual sampling locations

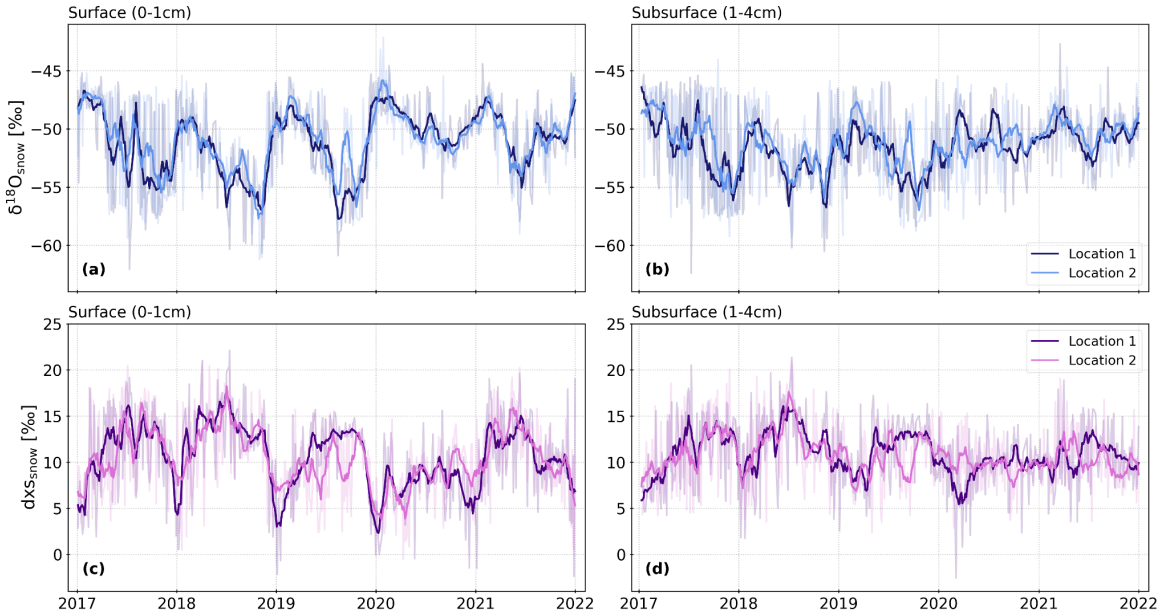

Figure S2. Snow isotopic compositions of the two samples collected 50 m apart (locations 1 & 2). Panels (a) and (b) show the time series for the snow surface and subsurface $\delta^{18}O$, respectively. Panels (c) and (d) show the time series for the snow surface and subsurface d-excess, respectively. In all four panels, the thin lines represent the original timeseries and the thick lines show the 30-day running means.

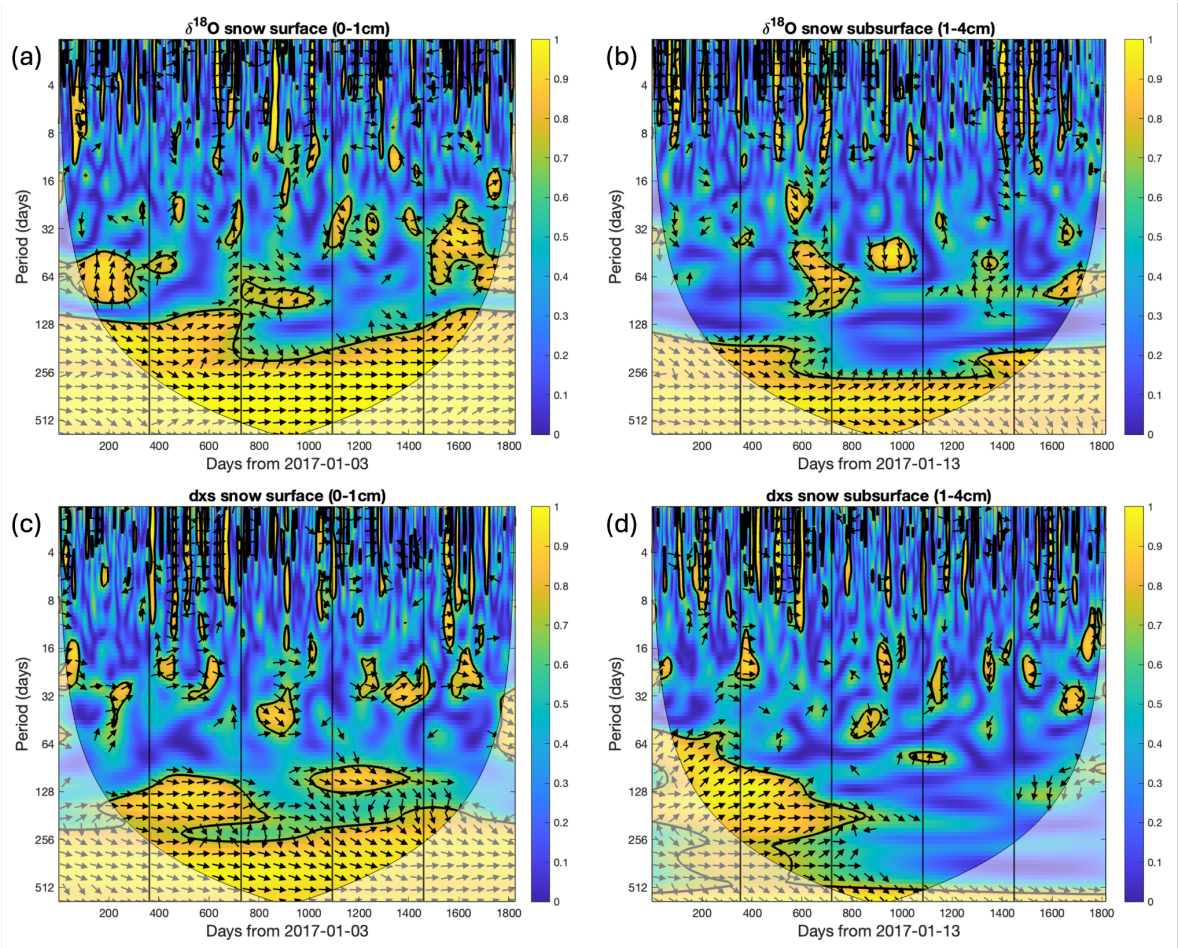

Figure S3. Squared Wavelet Coherence analysis between the two isotopic composition time series of the samples collected 50 m apart (locations 1 & 2) using the procedure of Grinsted et al. (2004). Panels (a) and (b) show the analysis for the snow surface and subsurface $\delta^{18}O$, respectively. Panels (c) and (d) show the analysis for the snow surface and subsurface d-excess, respectively. In all four panels, the 5% significance level against red noise is shown as a thick contour. The light white shade shows the cone of influence where edge effects might distort the picture. Arrows indicate phasing (angle corresponds to phase behaviour). The vertical black lines represent the first day of each year in the 5-year time series. Note that we linearly interpolated the four time series to daily time steps to be able to perform the analysis.

S4 Inputs to SISG model and simulations results

S4.1 Isotopic composition of precipitation

Figure S2 shows the comparison between the observed isotopic composition of precipitation (daily samples collected at Dome C) and the three artificial time series used as inputs to the SISG model.

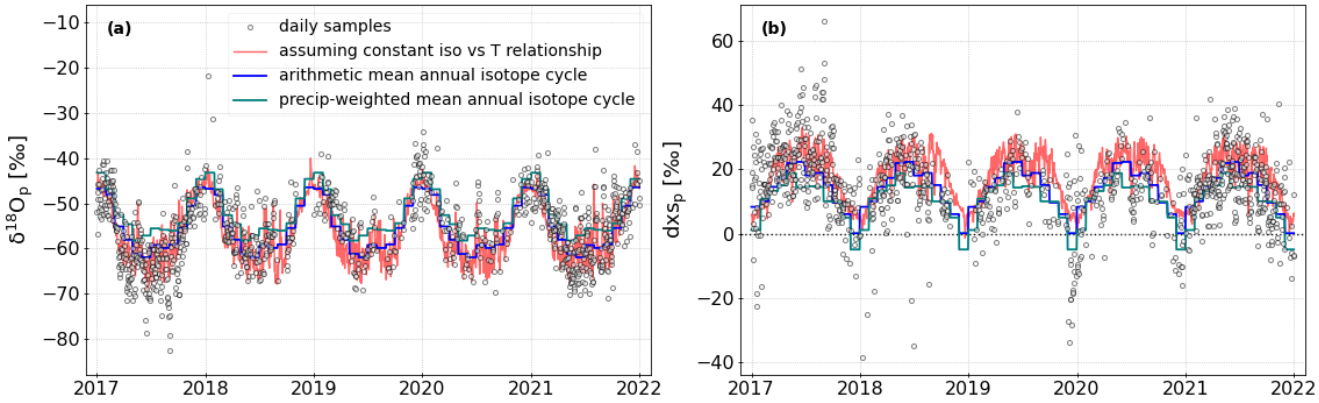

Figure S4. Comparison between the precipitation $\delta^{18}O$ (a) and d-excess (b) in the daily samples collected at Dome C (circles) and the three artificial time series of the precipitation isotopic composition based on the atmospheric temperature (red), the precipitation-weighted mean annual isotope cycle (blue-green) and the arithmetic mean annual isotope cycle (blue).

S4.2 Mean isotopic composition of observed and modelled snow layers

Table S2 summarizes the mean isotopic composition (over the five-year period 2017-2021) of the observed and modelled (five experiments with the SISG model) surface and subsurface snow layers.

Table S2. Mean isotopic composition of the observed and simulated snow surface over 5 years ($\delta^{18}O$ in normal font, d-excess in parenthesis and italic).

	Observations	"Iso from T & cst accu"	"Iso from T & ERA5 accu"	"Iso from wg. mm & obs accu"	"Iso from ar. mm & obs accu"	"Iso from ECHAM6 & ECHAM6 accu"
Surface layer (‰)	-51.0 *(10.4)*	-56.1 *(17.4)*	-53.1 *(13.9)*	-53.0 *(11.1)*	-55.7 *(14.0)*	-45.8 *(5.0)*
Subsurface layer (‰)	-51.4 *(10.8)*	-56.3 *(17.5)*	-53.4 *(14.2)*	-53.8 *(12.1)*	-56.8 *(15.5)*	-45.5 *(5.1)*

S4.3 Sensitivity tests on sample depths in the SISG model

We performed the experiment "iso from T and ERA5 accu" (isotopic composition of precipitation calculated from the atmospheric temperature and precipitation amounts from ERA5) with varying the surface and subsurface samples depths: 0-0.5 cm and 0.5-3.5 cm, 0-1.5 cm and 0.5-4.5 cm, 0-2 cm and 2-5 cm, 0-3 cm and 3-6 cm. The reference depths are 0-1 cm and 1-4 cm. In the current version of the model, the samples depths cannot overlap. The linear regression slopes (a) and RMSE between all modelled and observed monthly means $\delta^{18}O$ and d-excess in the five-year period are summarized in Table S3.

Table S3. Linear regression slope (a) and RMSE between the observed and modelled monthly mean isotopic composition of the subsurface layer ($\delta^{18}O$ in normal font, d-excess in parenthesis and italic) for different sample depths in the model. All linear slopes are significant (p-value < 0.05), except the ones marked with an asterisk (*, p-value > 0.05).

	Depths	0-0.5-3.5 cm	**0-1-4 cm (ref)**	0-1.5-4.5 cm	0-2-5 cm	0-3-6 cm
Surface layer	a	1.1 *(1.1)*	**1.2 *(1.0)***	1.1 *(0.8)*	1.0 *(0.6)*	0.8 *(0.3)*
	RMSE (‰)	4.4 *(5.6)*	**3.7 *(5.3)***	3.3 *(5.1)*	3.1 *(5.1)*	3.0 *(5.1)*
Subsurface layer	a	1.0 *(0.6)*	**0.8 *(0.2*)***	0.6 *(-0.2*)*	0.4* *(-0.6)*	-0.1* *(-1.0)*
	RMSE (‰)	3.0 *(4.6)*	**3.2 *(5.1)***	3.6 *(5.5)*	4.0 *(5.9)*	4.4 *(6.2)*

S4.4 Time span corresponding to samples depths

We retrieve from the SISG model the period of precipitation corresponding to the snow samples depths (0 to 1 cm depth for the surface layer and 1 to 4 cm depth for the subsurface layer) for different daily precipitation amounts (constant, observed, from ERA5 and from ECHAM6-wiso simulations). The period corresponds to the number of days necessary to build the snow layers. It assumes that the snowfall events are deposited on top of each other without any removal or redistribution and doesn't include the effect of snow compaction.

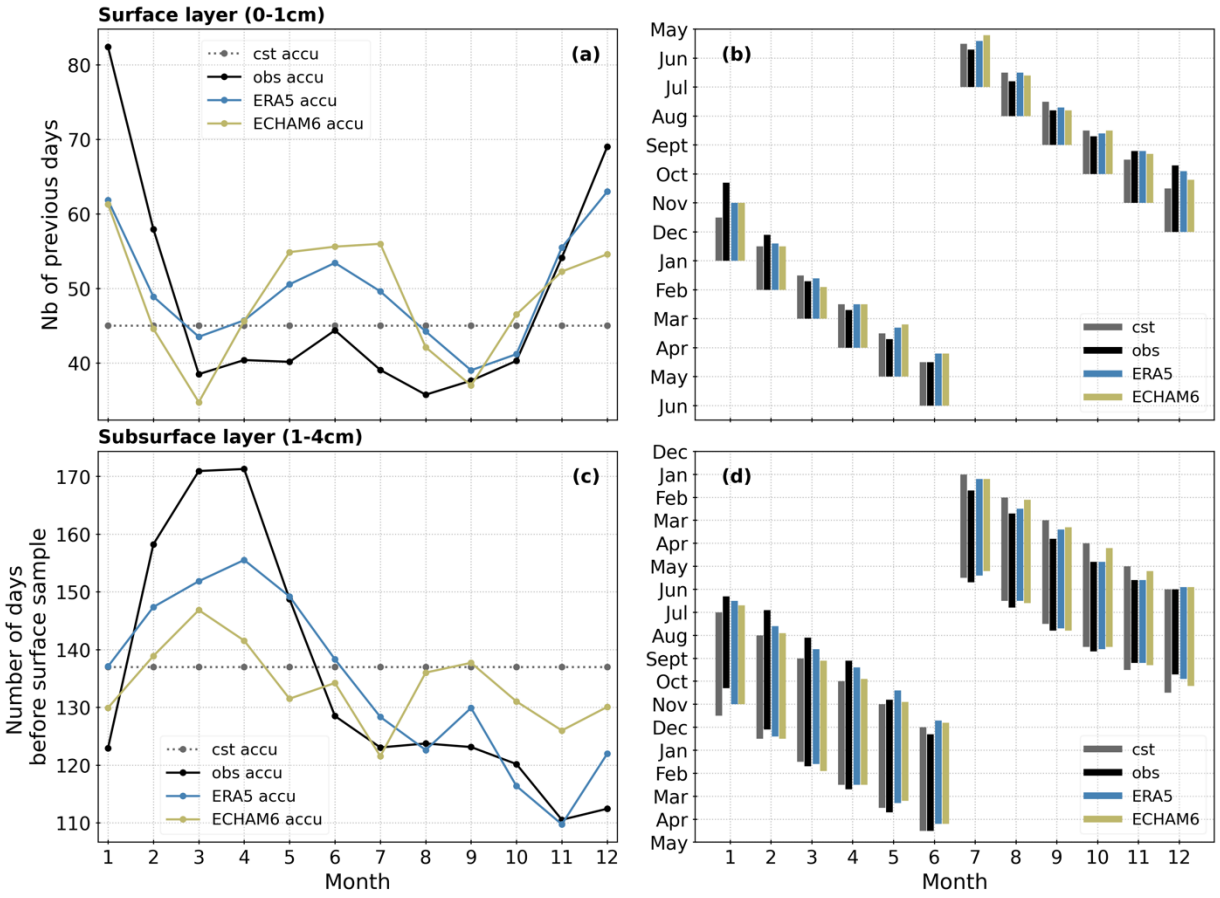

Figure S5. Average time span necessary to build the snow samples (0-1 cm for the surface and 1-4 cm for the subsurface), depending on the daily precipitation amounts. Panel (a) shows the mean (over the five-year period 2017-2021) number of days necessary to build a snow layer 1 cm thick (i.e. number of days "included" in the surface sample). Panel (c) shows the mean number of days necessary to build the subsurface layer (1-4 cm depth, excluding the surface sample). Panels (b) and (d) show which months are included in each snow layer. For example, a snow surface sample taken at the beginning of January integrates, on average over five years, precipitation events fallen in

November and December prior to sample collection (using ERA5 precipitation amounts). A subsurface sample taken at the beginning of January integrates precipitation events fallen between June and October prior to sample collection.

S5 Snow isotopic composition and wind speed

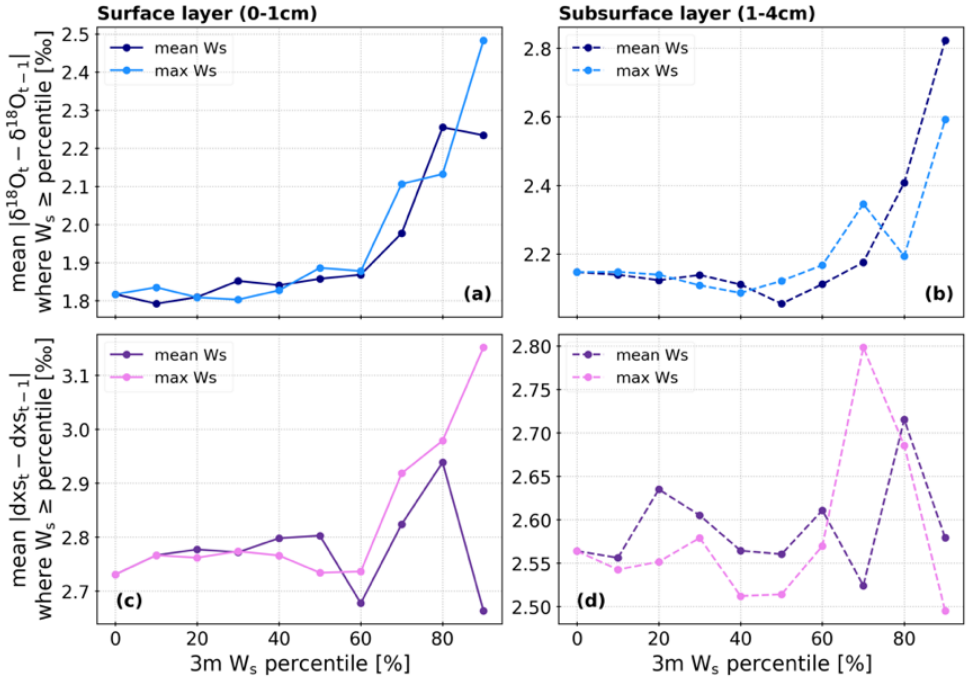

Figure S6. Average difference in $\delta^{18}O$ (a, b) and d-excess (c, d) between two consecutive sampling of the snow surface (a, c) and subsurface (b, d) during periods where the mean (and maximum) wind speed at 3 m is above a certain percentile. Wind percentiles are calculated over the whole 2017-2021 period.

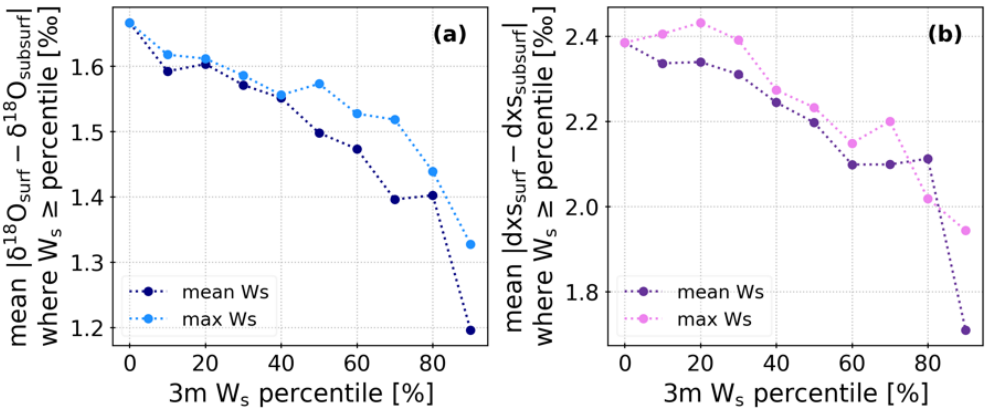

Figure S7. Average difference in $\delta^{18}O$ (a) and d-excess (b) between snow surface and subsurface during periods where the mean (and maximum) wind speed at 3 m is above a certain percentile. Wind percentiles are calculated over the whole 2017-2021 period.

S6 Precipitation isotopic composition versus precipitation amounts

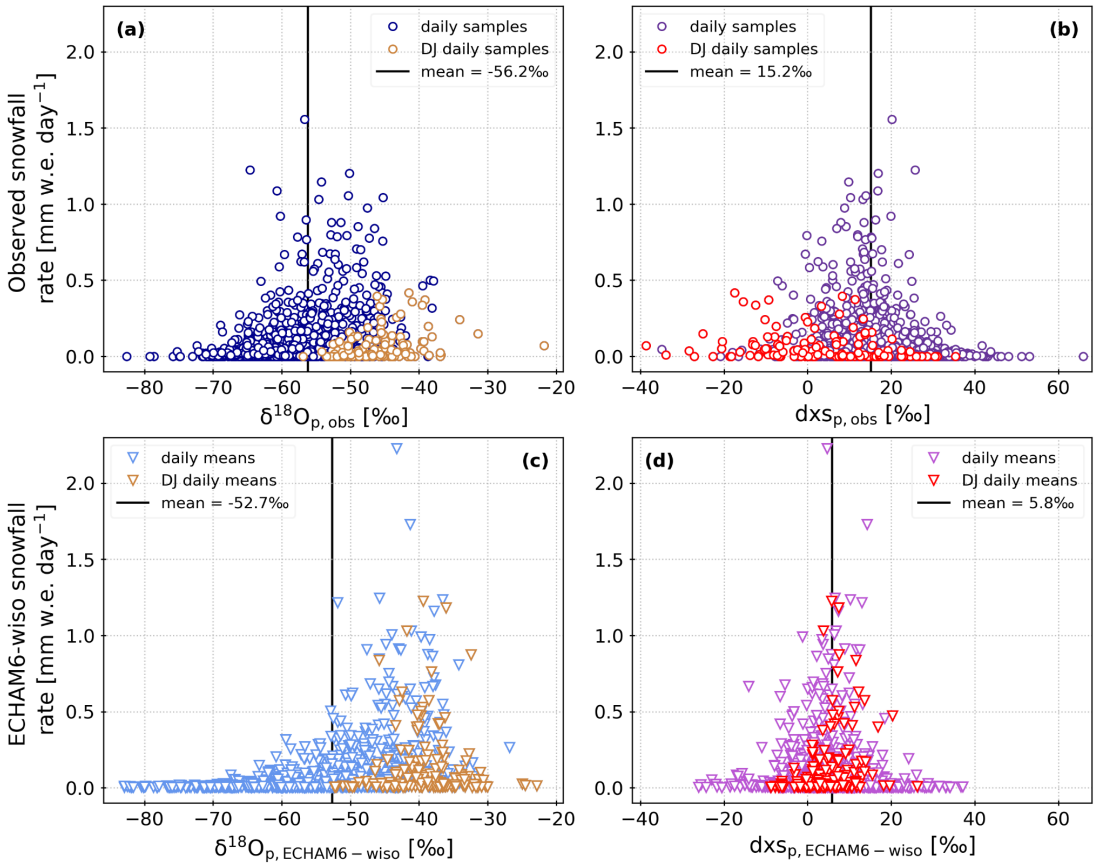

Figure S8. Daily precipitation isotopic composition ($\delta^{18}O$ in panels (a) and (c), d-excess in panels (b) and (d)) versus daily precipitation amounts, for the observations in panels (a) and (b) and the ECHAM6-wiso outputs in panels (c) and (d). In all four panels, the solid black line shows the mean isotopic composition of daily precipitation and the coloured markers (brown in panels (a) and (c) and red in panels (b) and (d)) show the days in December and January.

References for supplementary materials

Bretherton, C. S., Widmann, M., Dymnikov, V. P., Wallace, J. M., and Bladé, I.: The Effective Number of Spatial Degrees of Freedom of a Time-Varying Field, J. Climate, 12, 1990–2009, https://doi.org/10.1175/1520-0442(1999)012<1990:TENOSD>2.0.CO;2, 1999.

Genthon, C., Piard, L., Vignon, E., Madeleine, J.-B., Casado, M., and Gallée, H.: Atmospheric moisture supersaturation in the near-surface atmosphere at Dome C, Antarctic Plateau, Atmos. Chem. Phys., 17, 691–704, https://doi.org/10.5194/acp-17-691-2017, 2017.

Genthon, C., Veron, D. E., Vignon, E., Madeleine, J.-B., and Piard, L.: Water vapor in cold and clean atmosphere: a 3-year data set in the boundary layer of Dome C, East Antarctic Plateau, Earth Syst. Sci. Data, 14, 1571–1580, https://doi.org/10.5194/essd-14-1571-2022, 2022.

Grinsted, A., Moore, J. C., and Jevrejeva, S.: Application of the cross wavelet transform and wavelet coherence to geophysical time series, Nonlin. Processes Geophys., 11, 561–566, https://doi.org/10.5194/npg-11-561-2004, 2004.

Murphy, D. M. and Koop, T.: Review of the vapour pressures of ice and supercooled water for atmospheric applications, Q. J. R. Meteorol. Soc., 131, 1539–1565, https://doi.org/10.1256/qj.04.94, 2005.

Vignon, E., Raillard, L., Genthon, C., Del Guasta, M., Heymsfield, A. J., Madeleine, J.-B., and Berne, A.: Ice fog observed at cirrus temperatures at Dome C, Antarctic Plateau, Atmos. Chem. Phys., 22, 12857–12872, https://doi.org/10.5194/acp-22-12857-2022, 2022.